Published in the Proceedings of the 16th International Aluminum Alloys Conference (ICAA16) 2018
ISBN: 978-1-926872-41-4
by the Canadian Institute of Mining, Metallurgy & Petroleum

JOINING OF STEEL AND ALUMINUM BY MEANS OF FRICTION STIR WELDING PROCESS

*Sazol Das, Hany Ahmed, Ganesh Bhaskaran, and Zhuoru Wu

Novelis Inc,
Kennesaw, GA USA
*(*Corresponding author: sazol.das@novelis.adityabirla.com)*

ABSTRACT

Friction stir welding (FSW) process in lap configuration for dissimilar materials has been developed and tested for steel to aluminum joining. A novel cylindrical tool was designed for improved material flow. The joining of steel to high strength 5xxx and 6xxx aluminum was carried out by FSW technique using optimized process parameters. The microstructure, micro-hardness, joint strength and corrosion properties at the weld interface have been investigated. Optical and scanning electron microscopy reveled a well layered structure at the interface and lap shear tests of the welds showed excellent fracture resistance. Neutral salt spray tests for up to 500 hours (ASTM B117) were carried out on the bare steel to aluminum FSW joints, which did not show neither evidence of corrosion at the weld interface, nor any degradation of the weld strength. The FSW lap configuration was applied to prototype commercial vehicle structural component whereby a steel stiffener insert was friction stir welded to high strength 6xxx aluminum alloy. The interface microstructure showed layered root without any steel shattering in aluminum side. A finite element study was carried out to quantify the benefits where it was found that the stiffness increases by 76% under bending loads and 36% in torsion loads.

KEYWORDS

Friction stir welding, Dissimilar materials joining, Aluminum, Steel, Intermetallics, Lap joint, Joint strength, Weld microstructure, Stiffener, Corrosion, Finite element modeling

INTRODUCTION

Energy preservation and environmental issues, namely carbon footprint and legislation around emission in transportation industries has led to a growing need to use of lightweight materials such as aluminum and magnesium alloys along with various grades of steel in structural application, while still maintaining their strength and crashworthiness. Assembling dissimilar materials within integrated structure is thus a stringent requirement related to optimum performance. In order to achieve an efficient technology of joining dissimilar materials such as aluminum to steel, it remains difficult to select an effective welding process for a given joint configuration. The use of aluminum in transportation industries for structural component is not exclusive in a design and is almost always used along with various steel grades for a mixed materials solution, thus dissimilar aluminum/steel lap joining is of great interest since this is widely used in the assembly of parts (e.g. pillar, frame rails, chassis, body in white (BIW), CAB, etc.).

Dissimilar fusion welding between aluminum alloys and steel is a challenging process due to large difference in melting temperature and also the physical and mechanical properties of the alloys involved. The process results in inhomogeneous microstructure at the joint along with segregation due to limited solubility of Iron in Aluminum leading to the formation of brittle intermetallic (IMC) phases of Al_xFe_X, which are detrimental to the mechanical performance of the joint (Springer, 2011; Kubaschewski, 1982; Springer, 2011). Friction stir welding (FSW) is one of the most appropriate joining technique for dissimilar materials which involves plastic deformation in the solid-state without any bulk melting (Mishra, 2005; Nandan, 2008; Lohwasser, 2010). It is an art of the optimum joining technology of aluminum and other lightweight materials to steel, the technique is at an early stages of development. FSW process can plastically deform (stir) these dissimilar materials using simple welding tool made of tool steel. This solid state joining also reduces the occurrence of residual stresses, cracking, and porosity (Sato, 2004; Kimapong, 2004; Yan, 2005; Murr, 2010; Leitao, 2009; Kumbhar, 2011). The joining takes place with the movement of a rotating shouldered tool (made of tool steel) with a profiled pin plunged into the joint line between two piece of sheet or plate materials. The material is heated when the tool moves along the weld line by the friction produced between the shoulder of the tool and the work piece to be welded. Frictional heat causes the material to soften without reaching the melting point (Suhuddin, 2009; Xunhong, 2006). FSW is being used to joint dissimilar materials such as steel/aluminum alloys (Zadpoor, 2008; Uzun, 2005; Somasekharan, 2004; Park, 2003; Park, 2004; Thomas, 1999); however, there are challenges to produce good weld quality and ensure reproducibly, especially when it comes to joining thick gauge sheet for structural application.

In the present study efforts were made to produce FSW high quality joint between thick gauge (5–10 mm) 5xxx and 6xxx aluminum alloys to mild steel in lap configuration with varying tool rotational and traverse speed. The investigation also focused on overcoming the challenges such as residual stresses (warpage), creating integrated layered root structure free from IMC layers, wormhole steel shatters/debris and excessive metal flashing.

PROCEDURES AND EXPERIMENTS

Novelis Inc produced commercial 5xxx (6 mm) and 6xxx (10 mm) aluminum alloy plates that are suitable for structural and reinforcement parts in commercial vehicles were used in this study. Mild steel (1018) 2.3 mm pates were chosen to be joined to AA5083 – O and Advanz. S360T™ – T4 alloys using FSW. The chemical composition and mechanical properties of the alloys are shown in Tables 1 and 2, respectively. Both 5xxx and 6xxx alloys show a lower strength level compared to steel.

All the joints were produced in lap configuration since this is one of the most relevant joint configuration in structural application in commercial vehicles. FSW process were carried at the Edison Welding institute (EWI), OH, USA, using a commercial FSW instrument with various clamping and cooling condition. The welding setup is schematically illustrated in Figure 1. FSW tool made of AISI M42 tool steel consisting of a concave shoulder and domed pin tip with various probe features such as flats and threads was designed which was used for these welding configurations. All welds were conducted in position control rather than force control to achieve consistent tool penetration to the steel at the bottom of the lap configuration. Force control does not allow to maintain a consistent tool penetration throughout the weld

length which might affect the joint interface and root structure. Aluminum on top with a one inch overlap with steel and a 0.05–0.10 mm plunge into steel were used for the weld to avoid tool wear and steel shatters into the weld root. Tool rotation was maintained between 400–600 rpm with 80–160 mm/min traverse speed, while tool tilt angle with respect to vertical position was maintained at 2–3° with aluminum plate.

Table 1. Chemical compositions of the aluminum and steel alloys

Alloys	Si	Fe	Cu	Mn	Mg	Cr	C
AA5083	0.4–0.6	0.30–0.50	0.05–0.10	0.40–1.0	4.0–4.90	0.05–0.25	
Advanz. S360T™	0.50–1.2	0.20–0.30	0.70–1.00	0.05–0.20	0.70–1.20	0.01–0.15	
1018				0.60–0.90			0.14–0.20

Table 2. Typical properties of the aluminum and steel alloys used in the study

Alloys	Yield Strength (MPa)	Tensile Strength (MPa)	Elongation (%)	Density (g/cc)
AA5083 – O	115–125	275–350	25	2.65
Advanz. S360T™ – T4	130–160	240–260	25	2.70
1018	370	440	15	7.87

Joint strength of each trial was performed by pulling the welded strips using Instron™ tensile testing machine after water jet cutting to obtain the fracture load and extension before failure. Vicker micro-hardness testing was performed at the weld interface to determine the integrity and uniformity of the joint. The microstructure of the weld interface was investigated using Zeiss™ optical microscope (OM) and Philips XL – 30 scanning electron microscope (SEM) equipped with energy dispersive x-ray (EDXS). ASTM – B117 neutral salt spray was used to evaluate corrosion performance of the FSW joints. To simulate automotive painting conditions, the samples were subjected to Zn phosphated, with target coat weight of 2.5–3.0 g/m^2, followed by electrocoating in Cathoguard 500 (supplied by BASF). The coated samples were cured in the furnace maintained at 180°C for 20 min. For a base line comparison, the uncoated samples were also exposed in neutral salt spray test for 500 hours. Upon completion of the corrosion test, the residual strength of the joints were assessed using the Instron™ tensile testing machine and the macro images of delaminated surfaces were also examined to assess the integrity of the joint. Metallographic cross sections were done to ascertain the morphology of the corrosion attack at the weld interface. The FSW lap configuration was applied to a commercial vehicle's prototype structural component where a steel and aluminum stiffener insert was FSW to 6xxx aluminum alloy. The interface microstructure of the welded part was investigated using OM and SEM.

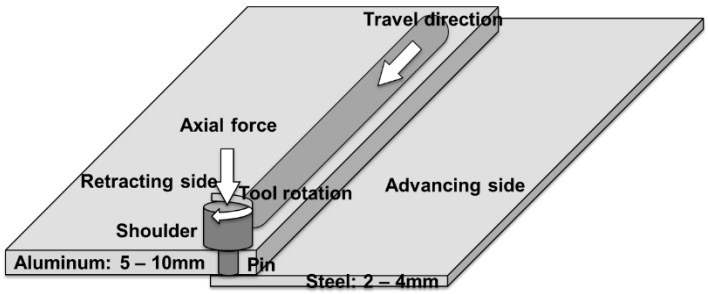

Figure 1. Schematic illustration of lap configuration used between Al and steel joint setup for FSW

A finite element (FE) study was carried out for the prototype component to quantify the benefit of the stiffener. The FE model was composed of a 410 mm side rail beam (10mm thickness) with two 2mm thick stiffener tied inside the structure. The material properties of Advanz. S360T™ in T6 temper with yield

strength of 330 MPa was applied to the side-rail beam. Two types of stiffener, Steel and Advanz. S360T™ – T6, were modeled to compare the loading conditions with no stiffener in the assembly as a base line standard. The model tested two loading conditions of 3-point bending and torsion as demonstrated in Figure 2. A 20 kN force and a 2 N.mm torque were used to induce the structure deformation in the elastic range only. Stiffness's and stresses were calculated for three conditions from the three structures of i) no stiffener as base line, ii) using a steel stiffener, and iii) using an aluminum stiffener.

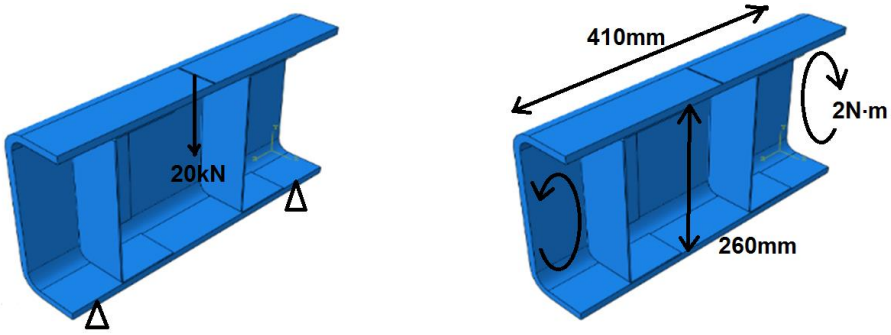

a) b)

Figure 2. Loading condition and boundary condition of the FE model: a) 3-point bending, and b) Torsion

RESULTS AND DISCUSSION

FSW process challenges for thick gauge dissimilar material joining along with detailed microstructural features, mechanical, corrosion and FE modeling data obtained from the study are summarized below with critical observations.

FSW Process Challenges

FSW process has various challenges in joining thick gauge dissimilar materials. The tool design is the most critical part that involves proper material flow and heat generation. Proper material flow depends on shoulder and probe profile. A concave shoulder can act as a material reservoir during the process and supply sufficient material to flow that avoid wormhole/void formation at the root of the weld. On the other hand proper thread and/or profile on the probe can lead to continuous material stirring. In the present study, a concave shoulder tool along with a probe containing thread and flat was designed to have proper material flow along with active stirring during the joining process.

The probe/pin tip was designed to be dome shaped to reduce stress concentration during the FSW process and increase the tip life. A dome shape tool also reduces the risk of steel shattering into the weld due to no sharp edge contact with the steel plate while stirring during the joining process. Heat generation is the main part of the FSW process that allows material to plastically deform in solid state which can be controlled by various process variables, such as tool rotational speed, tool traverse speed, axial /plunge force etc. Rotational speed mainly generate the frictional heat that helps stirring the material and also break any oxide layer that may be present on bare steel surface, whereas traverse/weld speed mainly act for heat dissipation and appearance of the weld. Axial/plunge force applied to the process to maintain proper contact during the process that also contribute to frictional heat generation. Tilt angle is another process variable that determines weld thinning and appearance of the weld. The AISI M42 FSW tool along with schematic illustration of the plunge depth is shown in Figure 3.

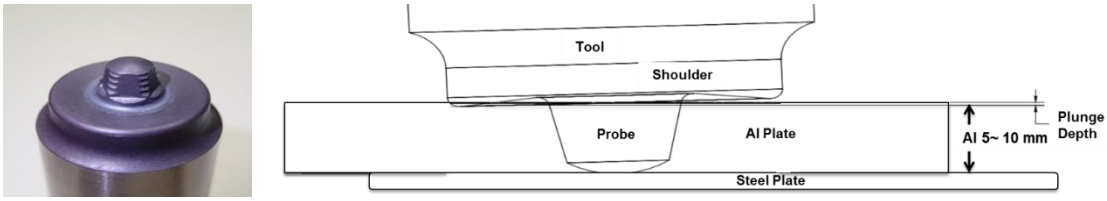

a) b)

Figure 3. FSW tool and lap configuration with plunge depth, a) FSW tool, and b) Schematic illustration

FSW tool probe length and diameter were varied depending on the aluminum plate thickness to maintain better contact, whereas the shoulder diameter was kept smaller to maintain less frictional heat during the process. Excessive flashing was observed during the first few weld due to movement of the plate during the FSW process for high rotational and axial force. Clamps were installed one inch apart on the sides to hold the plate along with two clamps at both end of weld start and finish to get a rigid structure which helped keep the plate in right place during the FSW process and minimize excess metal flashing.

A large amount of frictional heat produced during the thick gauge dissimilar material FSW process led to thermal expansion that is different for steel compared to aluminum. Thus, thermal contraction after the process has led to distortion/warpage at the joint which was challenging to mitigate with conventional FSW process. Enhanced cooling system was used during FSW to avoid distortion/warpage after the process. A forced air nozzle was connected to the back of the tool to cool the aluminum plate immediately after the weld and a copper plate anvil was installed at the bottom of the assembly to act as a heat sink from the steel plate which took care of the distortion. Water mist was also used for rapid cooling of the weld joint by using nozzle behind the tool which results in oxidation/rust formation at the weld interface that led to corrosion issues which discussed later part of this article. Figure 4 shows the clamping conditions and enhanced cooling system used in the current process to attain a sound weld joint in a lap configuration.

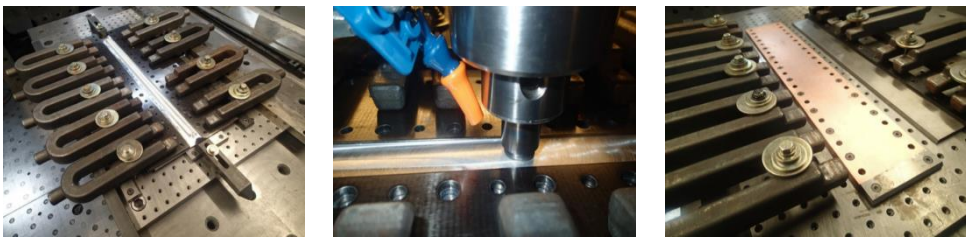

a) b) c)

Figure 4. FSW welding process setup, a) Clamping condition, b) Force air cooling, and c) Copper anvil

Microstructural Observations

All welds were cross-sectioned, mounted and polished to observe the weld root integrity at the interface. Figure 5 shows the interface microstructure at various weld parameters. High rotational speed could lead to excessive steel shattering at the interface (Figure 5a) and also the formation of thick Al_xFe_X IMC layer that is brittle in nature which adversely affects the weld mechanical properties. These steel particle can act as local galvanic cell and initiate corrosion under service condition. The brittle IMC layer also decrease the interface bond strength resulting in a low life cycle on the bond strength at service condition (Kimapong, 2005). High traverse speed on the other hand could increase the productivity, however it could also result in weld defects at the interface in terms of void and wormholes formation due to less time to stir the material at the root (Figure 5b). Optimum rotational speed is required to get proper frictional heat generation that could lead to good layered structure at the root without any steel shatters to achieve a mechanical interlock at the interface while maintaining productivity (Kimapong, 2005; Elrefaye, 2005; Movahedi, 2011). On the other hand a decent weld speed is required to have proper material flow at the root

without any void or wormholes. Figure 5c shows a well layered interface root without any steel shattering and free of voids by controlling the rotational and traverse speed of the tool during FSW process. The layered stirred structure and mechanical interlock at the weld interface will enhance the bond strength, while the part is in service condition.

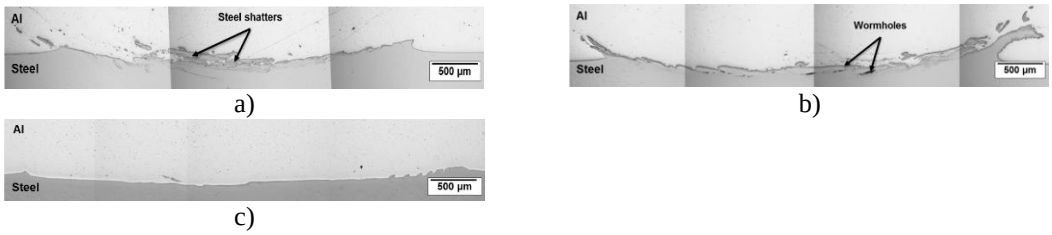

Figure 5. OM micrographs of weld cross-sections at the interface, a) Excessive steel shattering, b) Wormhole at the weld root, and c) Layered root

SEM was used to determine the IMC layer thickness and extent of steel shatter at the interface of the welds in backscattered electron (BSE) mode. EDXS point analysis was also performed to determine elemental composition of the IMC layer and scatter particles at the interface. Figure 6 shows the interface microstructure observed under SEM for couple welds to differentiate the IMC layer and steel shatters at the weld. The dark grey region in Figure 6a shows IMC layers in contrast to steel (light grey) and aluminum (dark). Figure 6b showing a stirred structure with a thin IMC at the middle of the root without any steel shattering.

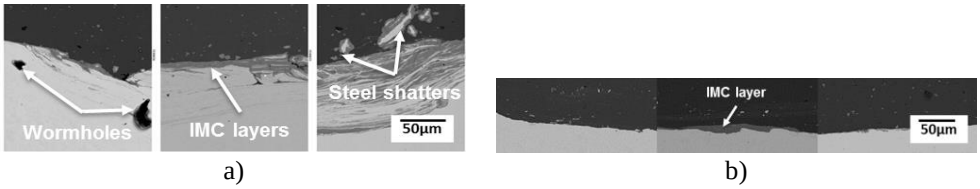

Figure 6. SEM images of weld cross-sections at the interface in BE contrast, a) excessive steel shattering with thick IMC layer, and b) thin IMC layer free of steel shattering

Mechanical Properties

Vickers microhardness (VHN) were taken at the weld interface on aluminum side to determine weld integrity (e.g. evidence of steel shattering and wormhole) with mounted cross-section. VHN is also a measure of weld stirred zone (SZ) and any thermo-mechanically affected zone (TMAZ) that may be introduced during FSW process. Fig 7a shows VHN profiles along the weld root for the welds where weld 13 and 14 showed higher VHN number in the middle of the root that represents steel shattering.

No noticeable change in VHN observed between SZ, TMAZ vs. base metal was observed which confirms the advantage of the FSW process. Optimizing the rotational and traverse speed reduced and minimize steel shattering to obtain good layered weld root with uniform VHN throughout the joining line. Joint strength were measured for the FSW assemblies as shown in Figure 7b for various process parameters. Weld 12 - 13 showed lower bond strength due to high rotational and traverse speed that produced steel shatter and IMC layer which deteriorates the bond strength (Figure 5a, 5b and 6a). Previous work also reported that higher rotational and traverse speed result in steel shatter and thick (≥ 5 µm) IMC layer which reduces the bond strength by 5–10% (Kimapong, 2005). Weld 15–16 showed good weld strength by reducing the rotational speed by 20% and traverse speed by 5% which eliminates any steel shatters and thick IMC (Figure 5c and 6b). It is worth noting that 70% of the joint strength was attained compared to the baseline metal strength for all the FSW bonded joints.

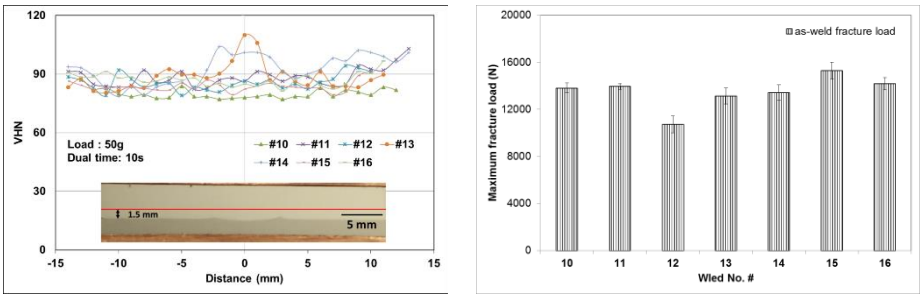

a) b)

Figure 7. a) VHN profile along the weld root along with the approximate location of measurement, and b) Fracture load at the interface for FSW joints represents bond strength

Corrosion Performance

The residual strength of weld 12 showing the lowest strength even in the case of painted variant (Figure 8). The macro images of the delaminated sample clearly shows the higher degree of rust compared to other weld schedule (Figure 9a). This could be associated with the movement of the water into the matting surfaces during FSW trial associated with the spray of the water mist for enhanced cooling. The cross sectional images (Figure 10a) also indicates that the contact between the steel and aluminum was not established robustly. These factors could have resulted in the reduced strength of the joints. In the weld schedule where the rotational speed of the tool was lowered, the steel particle appears to have shattered into aluminum matrix which might be a result of higher plunge depth. However, the degree of the shattering appears to be lower compared to welds with higher tool rotational speed. When these samples were subjected to corrosion testing, the cross section images (Figure 10b) clearly shows that the aluminum was attacked relative to the steel debris. In the optimized trial conditions with lower tool rotational and travel speed with higher vertical force employing a copper anvil resulted in a sound weld (Figure 10c and d).

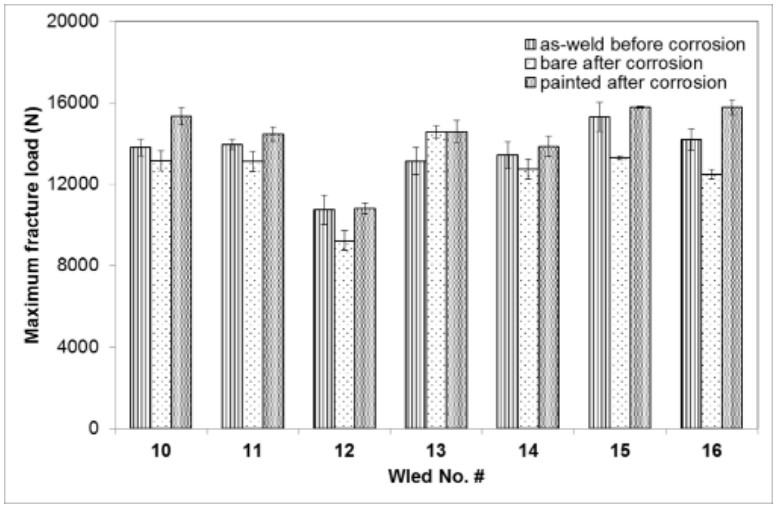

Figure 8. Fracture load at the interface for FSW joints represents bond strength

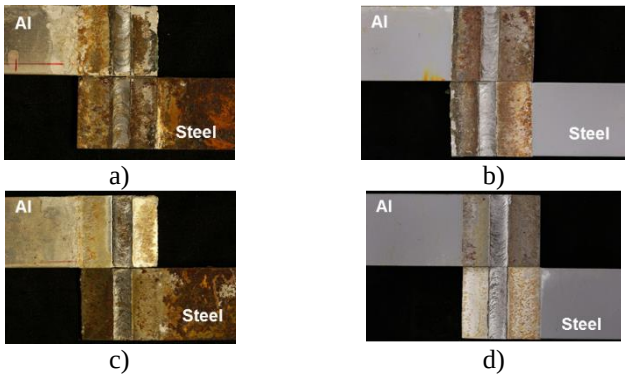

Figure 9. OM macrographs of weld interface after corrosion, a) Bare with water mist, b) Painted with water mist, c) Bare with force air and d) Painted with force air

The residual strength of the uncoated sample after corrosion testing was comparable to the as - welded sample. The cross section images didn't show any galvanic corrosion in the aluminum matrix and also no significant galvanic corrosion at the interface. The replacement of the water mist with the forced air appears to have reduced the extent of corrosion at the interface on the mating surface as well.

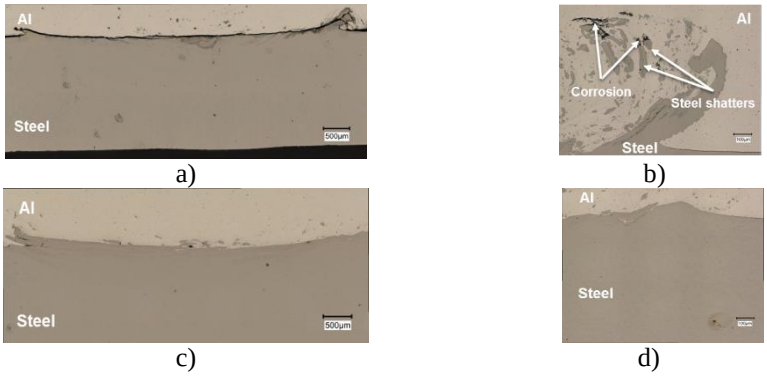

Figure 10. OM micrographs of weld interface at the cross-section after corrosion in bare condition, a) water mist, b) steel shatter, c) and d) optimum parameter

Finite Element Modeling

Three Point Bending

The applied loads for both the 3-point bending and torsion cases induced only elastic stresses in the structures. The Von Mises stress distribution of the 3-point bending for the three structures are shown in Figure 11. In the stiffener enhanced structures, the maximum stresses were found in the stiffeners where they shared part of the applied loading from the side-rail frame. It is clearly shown that the deformation of the stiffener enhanced structure were much lower than the base line structure with no stiffener inside. The steel stiffener displayed a better enhancement compare to the aluminum one. The stiffness values for frame rail without the stiffener followed by aluminum stiffener and steel stiffener were obtained as 1470, 1964 and 2594 N/mm respectively. Aluminum stiffener increased the stiffness of the assembly by 34% in 3-point bending model, whereas steel increased it to 76% to the original stiffness of the frame rail without stiffeners.

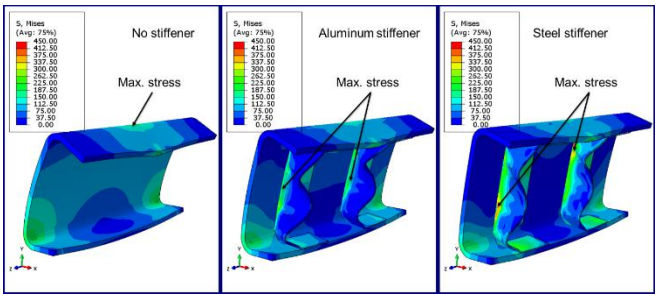

Figure 11. Stress distribution obtained from finite element modeling with no stiffener, aluminum and steel stiffener for 3-point bend loading

Torsion

Torsion simulation demonstrate similar trend as 3-point bending. The results are shown in Figure 12 where a 2 N.m torque was applied. Similar to 3-point bending, the stiffeners bear high stresses and highly reduced the stress of the side-rail frame. The torsional stiffness values for frame rail without the stiffener followed by aluminum stiffener and steel stiffener were obtained as 6.31, 7.33 and 8.58 Nm/rad respectively. Aluminum stiffener increased the torsional stiffness of the assembly by 16% whereas steel increased it to 36% to the original torsional stiffness of the frame rail. Both aluminum and steel stiffener joined using FSW process in lap configuration showed significant amount of improvement in stiffness and torsion which will allow the use of lightweight material in commercial vehicles structural component without compromising the performance.

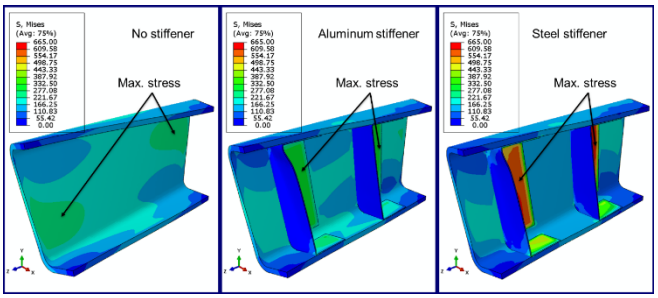

Figure 12. Stress distribution obtained from finite element modeling with no stiffener, aluminum and steel stiffener for torsion loading

CONCLUSIONS

A novel FSW tool was designed in Novelis Inc. with concave shoulder, domed tip along with flats and thread features on the probe for joining thick gauge dissimilar materials. The concave shoulder serves as material reservoir during the welding process. On the other hand profiles on the probe helped materials to reach the root of the weld to avoid weld defects. Both rotational and traverse speed contribute to the heat generation and IMC formation which determine the ultimate joint strength. Reducing rotational and traverse speed reduce the steel shattering and thick IMC formation, and also eliminates wormhole/void at the weld root. Adding enhance cooling system mitigate the large difference in heat expansion to avoid post weld distortion. However, the use of water mist produce oxidation at the interface results in delamination and lower interface strength. Using a forced air nozzle behind the tool along with a copper anvil at the bottom of the assembly provided best combination to avoid warpage/distortion after the weld. Steel debris and IMC also deteriorates the corrosion performance by creating local galvanic cell that initiate corrosion. Water mist showed higher corrosion rate at the interface due to presence of existing oxide layers. Bare samples after corrosion showed slightly lower bond strength compared to painted samples whereas painted samples maintained the strength similar to as-weld strength even after 500 h of neutral salt spray. An optimized

process parameter window for joining thick gauge dissimilar materials via FSW process was defined using the Novelis Inc. designed FSW tool. These optimized parameters were applied to a prototype structural component in a chassis of a commercial vehicle with steel/aluminum insert as stiffener to improve the stiffness and torsion performance of the component. Finite element model showed improvement after insertion of stiffener in aluminum structural component. The stiffness has increased by 34% for the assembly with aluminum and 76% for steel insertion respectively under bending loads. Whereas an increase of 16% and 36% in torsion has observed at the same configuration compared to the standard baseline frame rail without any stiffener.

ACKNOWLEDGMENTS

The authors would like to acknowledge the expert support from staff in the metallography, electron optics, electro-chemistry and mechanical testing laboratories at the Novelis Global Research and Technology Center (NGRTC). Authors would also like to acknowledge John Seaman and Beth Jackson in Edison Welding Institute for their help on performing all FSW welding trials at their facility at OH, USA.

REFERENCES

Elrefaey, A., Gouda, M, Takahashi, M., & Ikeuchi, K. (2005). Characterization of aluminum/steel lap joint by friction stir welding, *JMEPEG, 14,* 10–17.

Kimapong, K., & Watanabe, T. (2005). Lap Joint of A5083 Aluminum Alloy and SS400 Steel by Friction Stir Welding, *Mater. Trans. 46(4).* 835–841.

Kimapong, K., & Watanabe, T. (2004). Friction stir welding of aluminum alloy to steel, *Weld J. 83,* 277–285.

Kubaschewski, O. (1982). Iron-Binary Phase Diagrams, *Springer-Verlag, Berlin*.

Kumbhar, N. T., Sahoo, S. K., Samajdar, I., Dey, G. K., & Bhanumurthy, K. (2011). Microstructure and Microtextural Studies of Friction Stir Welded Aluminium Alloy 5052, *Mater. Des. 32(3).* 1657–1666.

Leitão, C., Emílio, B., Chaparro, B. M., & Rodrigues, D. M. (2009). Formability of similar and dissimilar friction stir welded AA 5182-H111 and AA 6016-T4 tailored blanks, *Mater. Des. 30,* 3235–3242.

Lohwasser, D., & Chen, Z. (Eds.) (2010). Friction Stir Welding: From Basics to Applications, Published by *Woodhead Publishing Limited and CRC Press LLC*.

Mishra, R. S., & Ma, Z. Y. (2005). Friction stir welding and processing, *Mater. Sci. Eng. R Rep. 50,* 1–78.

Movahedi, M., Kokabi, A. H., Seyed Reihani, S. M., & Najafi, H. (2011). Mechanical and microstructural characterization of Al-5083/St-12 lap joints made by friction stir welding, *Procedia Engg. 10,* 3297–3303.

Murr, L. E. (2010). A review of FSW research on dissimilar metal and alloy systems, *J. Mater. Eng. Perform. 19(8).* 1071–1089.

Nandan, R., DebRoy, T., Bhadeshia, H. K. D. H. (2008). Recent advances in friction-stir welding – process, weldment structure and properties, *Prog. Mater. Sci. 53(6).* 980–1023.

Park, H. S., Kimura, T., Murakami, T., Nagano, Y., Nakata, K., & Ushio, M. (2004). Microstructures and mechanical properties of friction stir welds of 60% Cu–40% Zn copper alloy, *Mater. Sci. Eng. A. 371,* 160–169.

Park, S. H. C., Sato, Y. S., & Kokawa, H. (2003). Effect of micro-texture on fracture location in friction stir weld of Mg alloy AZ61 during tensile test, *Scr. Mater. 49,* 161–169.

Sato, Y. S., Kurihara, Y., Park SHC. Y., Kokawa, H., & Tsuji, N. (2004). Friction stir welding of ultrafine grained Al alloy 1100 produced by accumulative roll-bonding, *Scr. Mater. 50*, 1233–1237.

Somasekharan, A. C., Murr, L. E. (2004). Microstructures in friction-stir welded dissimilar magnesium alloys and magnesium alloys to 6061-T6 aluminum alloy. *Mater. Charact. 52*, 49–64.

Springer, H., Kostka, A., Payton, E.J., Raabe, D., Kaysser-Pyzalla, A., & Eggeler, G. (2011). On the formation and growth of intermetallic phases during interdiffusion between low-carbon steel and aluminum alloys, *Acta Mater. 59(4).* 1586–1600.

Springer, H., Kostka, A., Dos Santos, J. F., & Raabe, D. (2011). Influence of intermetallic phases and Kirkendall-porosity on the mechanical properties of joints between steel and aluminum alloys, *Mater. Sci. Eng. A. 528*, 4630–4642.

Suhuddin, U. F. H .R., Mironov, S., Sato, Y. S., Kokawa, H., & Lee, C. H. (2009). Grain structure evolution during friction stir welding of AZ31 magnesium alloy, *Acta Mater. 57*, 5406–5418.

Thomas, W. M., Threadgill, P. L., & Nicholas, E. D. (1999). Feasibility of friction stir welding steel, *Sci. Technol. Weld. 4*, 365–372.

Uzun, C., Donne, C. D., Argagnotto, A., Ghidini, T., & Gambaro, C. (2005). Friction stir welding of dissimilar Al 6013-T4 to X5CrNi18-10 stainless steel. *Mater. Des. 26*, 41–49.

Xunhong, W., & Kuaishe, W. (2006). Microstructure and properties of friction stir butt-welded AZ31 magnesium alloy, *Mater. Sci. Eng. A. 431*, 114–117.

Yan, J., Xu, Z., Li, Z., Li, L., & Yang, S. (2005). Microstructure characteristics and performance of dissimilar welds between magnesium alloy and aluminum formed by friction stirring, *Scr. Mater. 53*, 585–589.

Zadpoor, A., Sinkeb, J., Benedictus, R., & Pieters, R. (2008). Mechanical properties and microstructure of friction stir welded tailor-made blanks, *Mater. Sci. Eng. A. 494*, 281–288.